

EXPERIMENTAL STUDIES OF OIL WITHDRAWAL FROM SALT
CAVITIES VIA FRESH-WATER INJECTION

Daniel C. Reda and Anthony J. Russo
Fluid and Thermal Sciences Department
Sandia National Laboratories, Albuquerque, New Mexico 87185

Abstract

The U.S. Strategic Petroleum Reserve (SPR) program coordinates the storage of crude oil in underground salt caverns. Oil removal from these caverns will be accomplished by injecting water into a brine volume located beneath the oil, buoyantly displacing the oil upwards, where it will then be recovered through a production pipe located near the top of the cavern. The critical question to be answered concerning this procedure was whether or not the crude oil would protect the salt walls from dissolution upon exposure to unsaturated brine following oil/brine interface passage. These oil/brine/salt interactions were experimentally investigated in the laboratory. Cylindrical cavities were created by machining (hollowing-out) salt cores from one end, leaving the circular wall and bottom as an integral piece. In each of four separate experiments, a salt cavity was placed vertically in a pressure vessel and its interior filled with crude oil overlying a saturated-brine "pocket". The vessel was sealed and pressurized to actual SPR-cavern pressure. Fresh water was injected down a tube and into the brine pocket, displacing the oil upwards, where it was recovered from the cavity through a second (production) tube near the top of the vessel. A traversable gamma-beam densitometer was positioned above the initial saturated-brine/oil interface and was used as a non-intrusive diagnostic to define the presence, or absence, of salt dissolution (cavity shape change) during the transient oil-withdrawal process. Such measurements showed the occurrence of salt-wall recession following interface passage in all tests, i.e., crude-oil adherence, and/or penetration, at the salt wall failed to protect the salt from dissolution upon its exposure to unsaturated brine. Measured post-test cavity shapes corroborated the transient results. Both transient and steady-state measurements were found to be in good agreement with numerical predictions generated via SANSMIC (the Sandia Solution-Mining Code) once the assumption of "no oil-layer protection" was invoked.

CONTENTS

| | <u>Page</u> |
|---|-------------|
| INTRODUCTION. | 9 |
| EXPERIMENTAL APPROACH | 13 |
| PRE-TEST RESULTS. | 22 |
| EXPERIMENTAL RESULTS. | 29 |
| COMPARISONS WITH NUMERICAL PREDICTIONS. | 41 |
| CONCLUSIONS | 45 |
| REFERENCES. | 46 |

FIGURES

| | | <u>Page</u> |
|-----------|--|-------------|
| Figure 1 | SPR Cavern Oil-Withdrawal Schematic | 10 |
| Figure 2 | Schematic of Experiment | 14 |
| Figure 3 | Gamma-Beam Densitometry, A Schematic | 16 |
| Figure 4 | Contrast Method for Electronics Calibration | 18 |
| Figure 5 | System Time-Constant Calibration. | 20 |
| Figure 6 | Oil-Penetration Tests | 23 |
| Figure 7 | Schematic of Predicted R(t) Responses | 26 |
| Figure 8 | Photograph of Gamma-Beam System and Test Vessel | 30 |
| Figure 9 | Photograph of Salt Cavity Model | 31 |
| Figure 10 | Measured Count-Rate Distribution, SPR2, t=0 | 34 |
| Figure 11 | Measured Transient Count-Rate Response, SPR2, X-10.03 cm. , | 35 |
| Figure 12 | Measured Count-Rate Distribution, SPR2, t=∞ | 37 |
| Figure 13 | Photograph of Post-Test, Sectioned, Salt Cavity for SPR2 | 38 |
| Figure 14 | Measured Post-Test Cavity Shape, SPR2 | 40 |
| Figure 15 | Transient Count-Rate Response, SPR2, Data versus Predictions. | 42 |
| Figure 16 | Post-Test Cavity Shapes, SPR2, Data versus Predictions | 43 |

TABLES

| | <u>Page</u> |
|--|-------------|
| Table 1 Summary of Test Conditions. | 32 |

NOMENCLATURE

| | |
|------------|---|
| d | beam diameter (cm) |
| I | unattenuated beam intensity after passage through material(s) (particles/sec) |
| I_o | unattenuated beam intensity at source exit (particles/sec) |
| a | average volumetric flowrate (cm ³ /min) |
| R | count rate (counts/sec) |
| r | cavity radius (cm) |
| t | time (min) |
| \bar{U} | average oil/brine interface velocity (m/hr) |
| X | vertical coordinate, measured from initial cavity bottom (cm) |
| X_γ | gamma-beam vertical coordinate, measured from platform zero location (cm); $X = X_\gamma - 5.84$ cm |
| z | coordinate measured along beam pathlength (cm) |
| δ | oil-layer thickness (cm) |
| ϵ | salt-wall recession (cm) |
| μ | gamma-beam linear attenuation coefficient (l/cm) |
| ρ | density (g/cm ³) |
| τ | electronics system time constant (μ sec) |

Subscripts

| | |
|-------|---|
| B | brine |
| f | final interface location |
| I | interface |
| i | initial interface location; of material i with μ or z |
| INJ | injection |
| o | oil |
| S | salt |

| | |
|----|------------------|
| SB | saturated brine |
| WD | withdrawal |
| | without contrast |
| 2 | with contrast |

INTRODUCTION

The United States Strategic Petroleum Reserve consists of an underground 011 storage system comprised of caverns which have been leached in salt domes located in the Gulf Coast states of Louisiana and Texas. Some of the cavern space, formed during commercial brining operations, was available for 011 storage shortly after the SPR program began in the mid-1970's. However, since the available volume was less than that required for the storage of 250 million barrels of 011, and a storage of up to one billion barrels was contemplated, the Department of Energy (DOE) undertook an extensive new cavern leaching program.

Since the end of 1978, Sandia National Laboratories has been serving as a technical consultant to the DOE on various aspects of the SPR program, including the cavern leaching and filling efforts. Early experimental and theoretical work on salt dissolution rates and salt cavity formation techniques¹⁻⁷ led to the development of three numerical models to predict solution mining processes⁷⁻⁹. Of these three, the computer code of Saberian⁷ was utilized early in the SPR program to help define initial cavern leaching schedules.

Because there was an urgency to form and fill the reserve as rapidly as possible, considerable attention was given to devising a leaching scheme which would yield not only the desired size and shape of cavern, but would do it in the shortest practical time. This appeared to be best accomplished by using a "leach-fill" strategy in which the cavern would be simultaneously filled with oil as the leaching proceeded. To start the cavern, several wells could be drilled and simultaneously leached until the cavities coalesced to form the final storage volume. The majority of the final volume would ultimately be filled with crude 011, overlying a small saturated-brine pocket located at the cavern bottom. 011 withdrawal from such caverns would be accomplished by injecting fresh water down a pipe to a level below the "initial" saturated-brine/oil interface, buoyantly displacing the 011 upwards, where it would then be removed through a production pipe whose entrance was located near the top of the cavern (see Fig. 1).

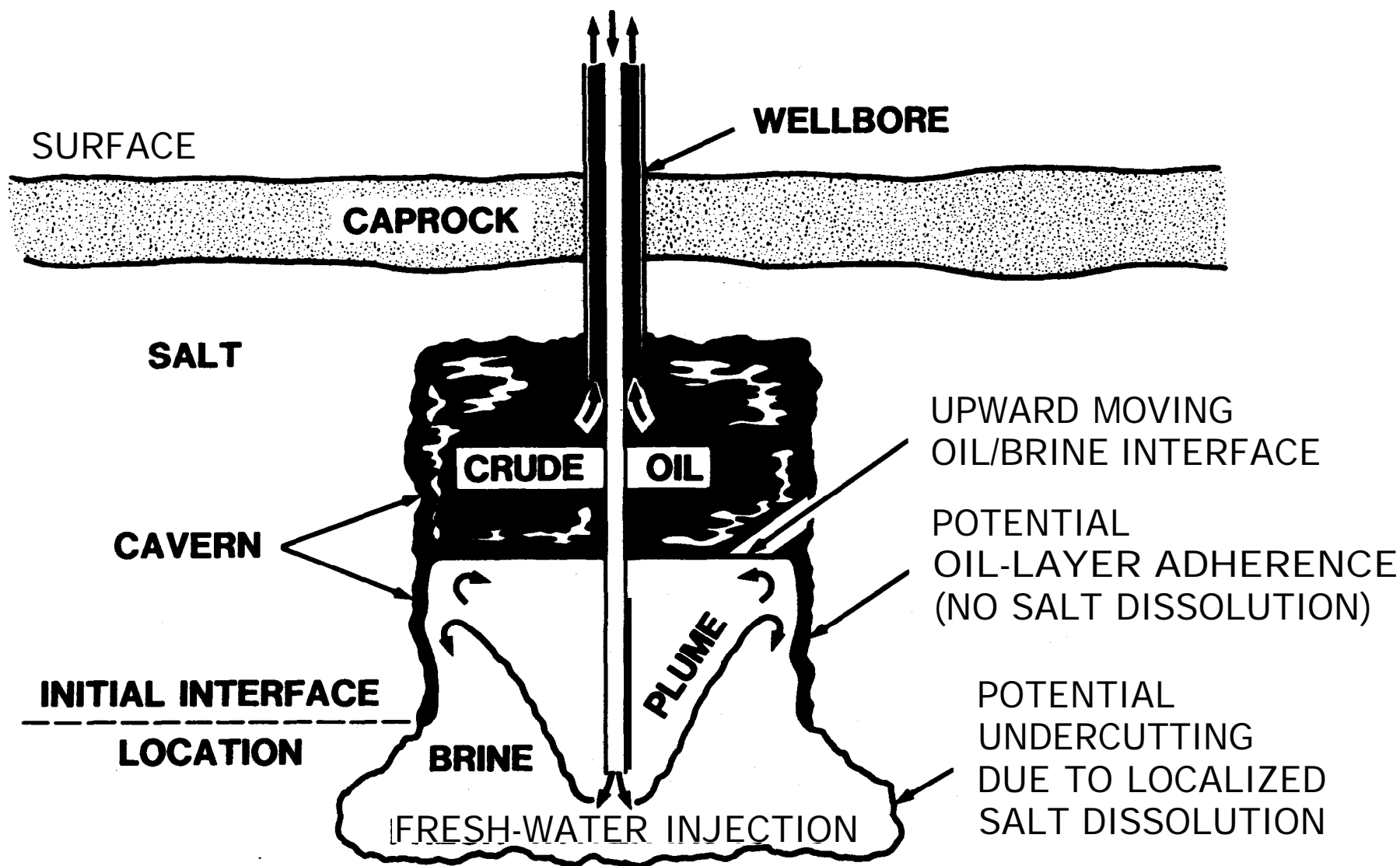


FIG. 1: SPR Cavern Oil-Withdrawal Schematic

Considering these leaching, filling, and withdrawal processes, it became apparent that there was a need to numerically model "moving interface problems" (i. e. , salt dissolution below an oil interface whose location varies with time). Since the *Saberian code*⁷ was not structured to treat such problems in an efficient manner, and since it would be necessary to perform a very large number of computer simulations of these various processes, a new code was developed^{10,11}. This code, called SANSMIC (the Sandia Solution-Mining Code), utilizes the same dissolution model as the *Saberian code*⁷, but it includes new diffusion, plume^{12,13}, and insolubles models. It also incorporates an implicit numerical formulation which significantly reduces computer run times. Cavern geometries are treated as two-dimensional/axisymmetric.

Cavern shapes predicted to occur during solution-mining operations were shown to be in favorable agreement with final cavern shapes measured via sonar caliper techniques"". It was noted, however, that for the oil-withdrawal option, "at present there is no way to evaluate (the code's) accuracy." This serious limitation stems from the fact that certain critical questions concerning the physics of oil/brine/salt interactions which occur during oil withdrawal have yet to be answered.

As was noted above, the planned oil-withdrawal procedure calls for fresh water to be injected into the cavern below the initial saturated-brine/oil interface. As this oil/brine interface rises, cavern surfaces formerly covered by oil become exposed to unsaturated brine. If these newly-exposed salt surfaces start to dissolve "immediately," the cavern will grow uniformly during each oil-withdrawal cycle. However, if the oil adheres to and/or penetrates the salt, thereby protecting it from dissolution, then only the lower portions of the cavern (which have never been oil covered) will undergo shape change. Highly abnormal ("undercut") cavern contours would thus result. This phenomenon could ultimately lead to coalescence of adjacent caverns, collapse of unsupported salt volumes, and surface subsidence problems.

Although oil-recovery procedures noted herein have been successfully demonstrated in the field (during short-time-duration tests), the quantity of oil temporarily removed from the SPR cavern was insufficient to allow **resolution of this critical** issue. To investigate such complex transient physical phenomena in a controlled and meaningful way in the laboratory would require that experiments be conducted using the materials of interest, subjected to conditions of interest, so as to most closely simulate the actual oil-withdrawal procedure. Furthermore, physical measurements should be made in a non-intrusive manner in order to avoid interfering with the fluid/solid interactions occurring in the near-wall **region**.

Such experiments were undertaken as the principle objective of the present research. In addition, salt cavity shape-change data were also obtained in an effort to further validate the **SANSMIC** code.

EXPERIMENTAL APPROACH

The first task in the present research was to formulate an experimental approach consistent with stated objectives. Figure 2 shows a schematic of the apparatus which resulted.

Salt cores were machined hollow from one end, leaving the circular wall and bottom as an integral piece. Nominal pretest dimensions were: OD = 9.17 cm, ID = 5.08 cm, cavity depth = 20.32 cm, and overall height = 22.86 cm. Each salt cavity was placed vertically in a pressure vessel with its open end at the top. The cavity interior was filled with crude oil overlying a saturated-brine pocket (details of pre-test procedures and test conditions will be given later). A thin (.013 cm) layer of saturated brine surrounded the external surfaces of the salt sample, providing a pressure-equilibration mechanism throughout the vessel interior upon pressurization.

The test vessel was pressurized from a commercially-available nitrogen bottle, the test pressure being maintained constant by a pressure regulator and adjustable bleed valve arrangement. The test pressure was transferred to the working fluids at a nitrogen/water interface in a separate pressure vessel.

Stainless steel tubing (ID = .079 cm) was used for the injection and withdrawal lines. For present tests, injection occurred at a vertical distance (X), measured from the cavity bottom, of 1.27 cm; withdrawal occurred at $X = 19.05$ cm. The injection line was preflooded with fresh water, and the exit line was preflooded with oil, prior to the start of each test.

A pre-calibrated flow-control valve on the exit line was opened to the desired vernier setting at the start of each transient, allowing oil to begin exiting the cavity as fresh water entered. Oil volumetric flowrate was continually monitored and the needle valve adjusted (if required) to maintain the exit flowrate constant. Total oil volume collected during the withdrawal time thus defined the average exit flowrate, \bar{Q}_{WD} .

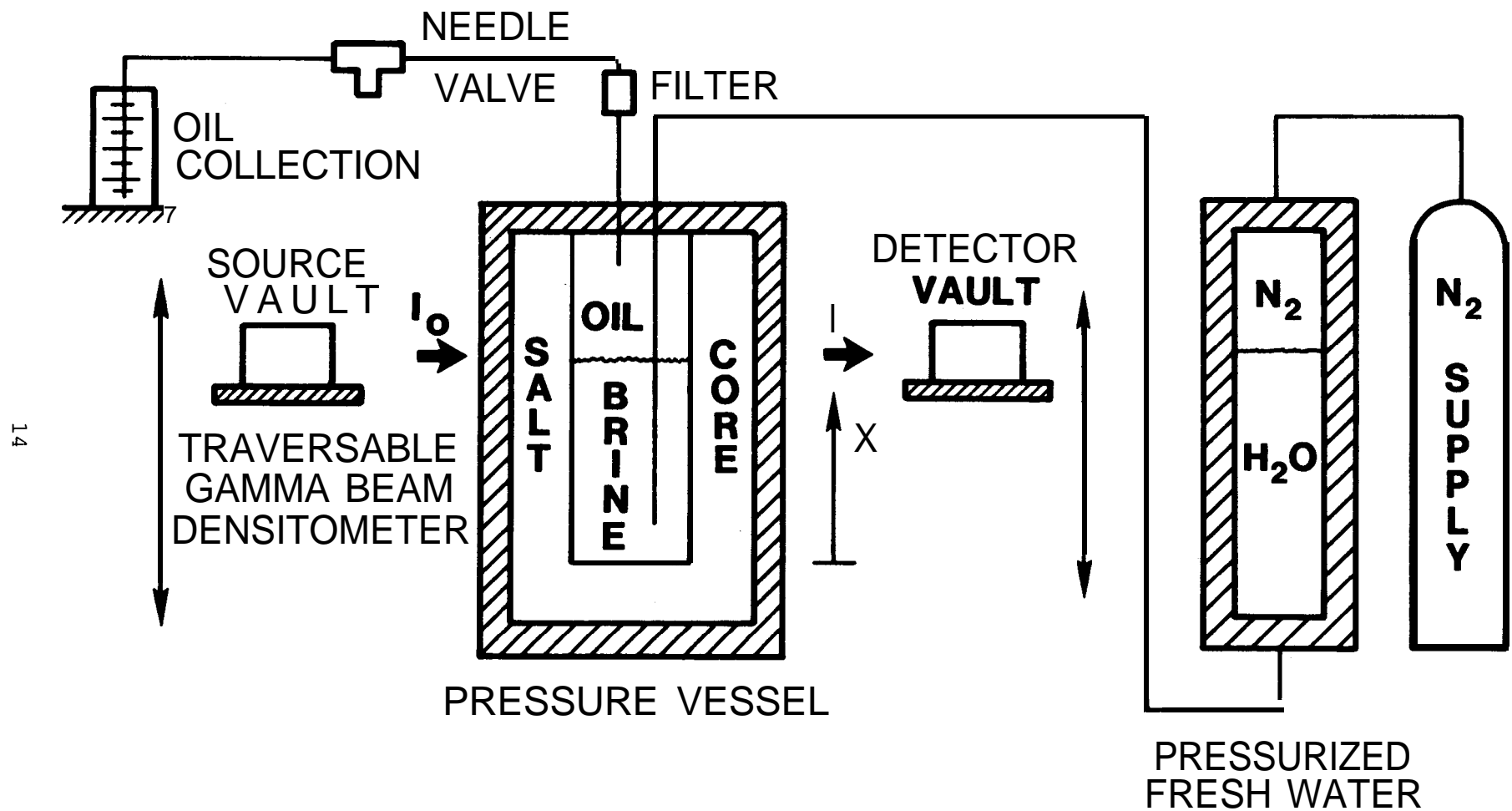


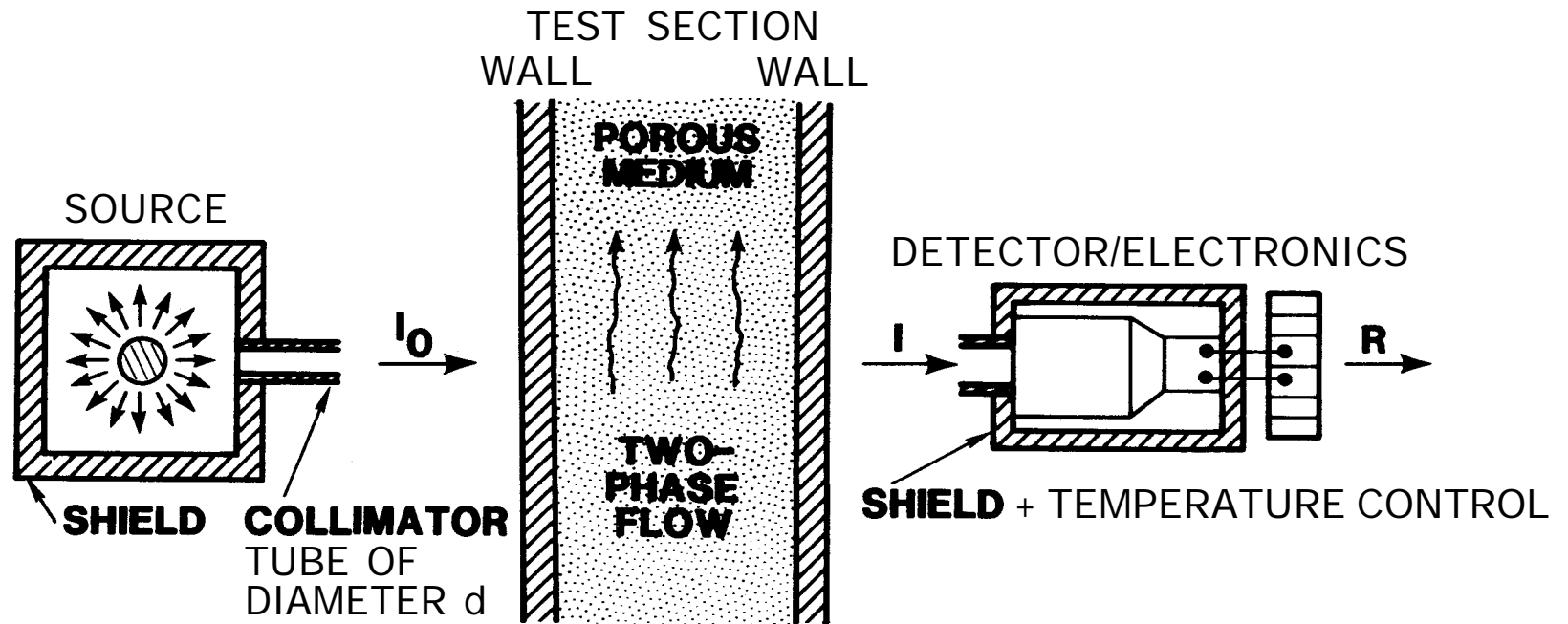
FIG. 2: Schematic of Experiment

At the completion of oil withdrawal, the water entry line was left "opened" in order to maintain the cavity at a constant pressure until equilibrium (saturated-brine) conditions were again achieved within the cavity (as measured with the instrumentation system described below). Overall change in liquid level (and thus volume) in the fresh-water reservoir was then measured with the following result, $\bar{Q}_{INJ} = 1.03 \bar{Q}_{WD}$. The non-equivalence of these two volumetric flowrates is due primarily to two competing mechanisms which occur throughout the entire oil withdrawal period, namely, water volumetric increases due to the addition of dissolved salt versus the slightly-larger volumetric increase of the cavity itself due to this same dissolution. (Minor factors which also contribute to this empirically-defined relationship are (1) dissolvable impurities in the salt, and (2) the constant-pressure post-withdrawal approach to equilibrium over a finite time period.) Theoretically, for dissolution of pure NaCl in pure H₂O, the constant of proportionality was calculated to be 1.03627.

Having defined the apparatus, it remained to select a viable instrumentation system which could be used to investigate the transient oil/brine/salt interactions inside a pressurized salt cavity in a non-intrusive manner. Gamma-beam densitometry, currently being applied at Sandia National Laboratories to study two-phase flows in porous media¹⁴, was chosen for use in the present experiment. In order to review the basic principles and components of this system, Fig. 3 was reproduced from Ref. 14. As will be shown below, this system was used to quantify the transient interactions, as well as to measure resultant cavity shape change.

A Cesium 137 pellet is housed in the source vault and emits gamma (γ) particles of energy 0.662 MeV. These particles exit the source vault through a collimator tube of diameter d. For a 5-curie source strength, and d = 0.318 cm, the initial (unshielded) beam intensity I_0 was measured to be $1.2527 \times 10^6 \gamma/\text{sec}$.

The interaction of gamma particles with matter is described by the exponential equation given in Fig. 3, where I is the beam intensity of unattenuated particles exiting the test chamber and $\mu_1 z_1$ is the product of



$$I_0 = I_0(d^2)$$

SPATIAL RESOLUTION = $f(d)$

$$I = I_0 e^{-\sum_{i=1}^n \mu_i z_i}$$

$$R = \frac{I}{(1 + \tau I)}$$

$$\tau = \tau(R)$$

FIG. 3: Gamma-Beam Densitometry, A Schematic

the total linear attenuation coefficient (μ_i) and the total integrated path length through which the beam must pass (z_i) for material i. The exit beam is comprised of both unattenuated particles at 0.662 MeV and particles which have been attenuated to lower energy states but are still in the beam path; attenuated particles physically scattered out of the beam path do not enter the detector collimator tube.

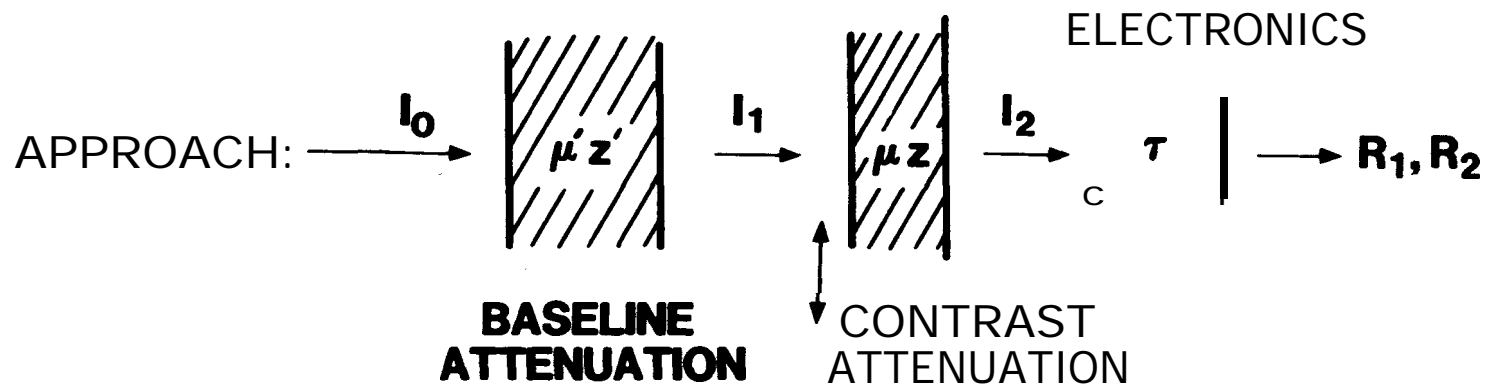
Gamma particles which enter the detector collimator tube strike a Sodium Iodide crystal and are converted into visible photons. These photons are detected by a photomultiplier tube which, together with a built-in preamplifier, send a voltage pulse to the counting electronics for each photon detected. The magnitude of this voltage pulse is proportional to the energy of the incoming gamma particle. A single-channel analyzer is then used to discriminate pulse height, yielding a count rate R (counts/sec) which is proportional to the intensity of unattenuated particles, I . At high particle fluxes, some pulses "overlap" in time and are subsequently lost to the counting electronics. The conversion of I into R is thus non-linear, being dependent on the characteristic time constant τ of the system (see equation in Fig. 3).

An improved calibration technique for $\tau(R)$, recently developed by Reda and Hadley to replace techniques reported earlier¹⁴, was used in this work. Figure 4 summarizes this new approach, referred to as the "contrast method." Intensity I_0 is reduced to intensity I , by some "baseline" attenuation (any material(s) may be used for this purpose). A corresponding count rate, R_1 , is then measured. The baseline intensity I , is then "contrasted" by some known-thickness "slab" of material (preferably of a known chemical composition, so that its theoretical μ value is known, thus supplying an independent check on measured results; e.g., pure water). A count rate, R_2 , corresponding to the contrasted intensity I_2 ($I_2 < I_1$) is then measured.

If one starts this procedure with a "sufficiently thick" pathlength of baseline material(s), I , and thus R_1 , will be small ($\approx 10^3$ counts/sec). In this limit, system "deadtime" goes to zero, i.e., $R_1 \rightarrow I$, and $R_2 \rightarrow I_2$, allowing μ for the contrasting material to be measured directly (see equation at the bottom of Fig. 4).

DEFINING EQS. :

$$\left\{ \begin{array}{l} I = I_0 e^{-\sum \mu_i z_i} \\ I = \left[\frac{R}{1 - \tau R} \right] \end{array} \right.$$



$$\text{DATA REDUCTION} = \tau = \frac{R_1 - R_2 e^{\mu z}}{R_1 R_2 [1 - e^{\mu z}]} \quad \text{FOR } (R_2 \leq R \leq R_1)$$

WHERE, $\mu = \frac{1}{z} \ln (R_1/R_2)$ **FOR LOW R**
(R \rightarrow I)

FIG. 4: Contrast Method for Electronics Calibration

By systematically reducing the thickness of the baseline material(s), and by repeating the above procedure, data over the entire count-rate regime of interest can be obtained. Algebraic manipulation of the two defining equations for the system yields an explicit equation for τ in the range $R_2 \leq R \leq R_1$, as a function of R_1 , R_2 and μz for the contrasting material (all quantities known). A "calibration" curve for $\tau(R)$ can then be generated by curve fitting the measured data (see Fig. 5; note, the horizontal bars on the data points define the $R_2 \rightarrow R_1$ range measured in each contrast test).

Measurement accuracy of the gamma-beam system is discussed below. Two effects introduce experimental uncertainties: (1) temperature variations in the system electronics (primarily in the crystal and the photomultiplier tube) can result in a "drift" of the mean signal, and (2) statistical variations in beam intensity (I_0) cause a superimposed random "noise" on the mean signal. Concerning the first effect, the entire laboratory was temperature controlled. In addition, the three components housed within the detector vault (i.e., the crystal, photomultiplier tube, and preamplifier) were wrapped by a cooling coil. Water from a constant-temperature bath was continuously circulated through this coil, maintaining thermal equilibrium. Concerning the second effect, repeated measurements (made under constant-attenuation conditions) showed maximum statistical variations in R to be ≈ 50 counts/second, consistent with error analyses¹⁴. Count rate variations experienced during various segments of the transient oil-withdrawal experiment were predicted (and ultimately measured) to be ≈ 500 to ≈ 5000 counts/second, i.e., well above the system maximum noise level. The gamma-beam system was thus proven to be a viable diagnostic technique for present applications.

The measurement capabilities of the single-energy/single-beam system can now be summarized. The count rate, R , resulting from beam passage through the test vessel is measured. Knowing $\tau(R)$ allows R to be converted to I . For a known I_0 , the exponential law then allows the determination of any one unknown μ_1 or z_i value.

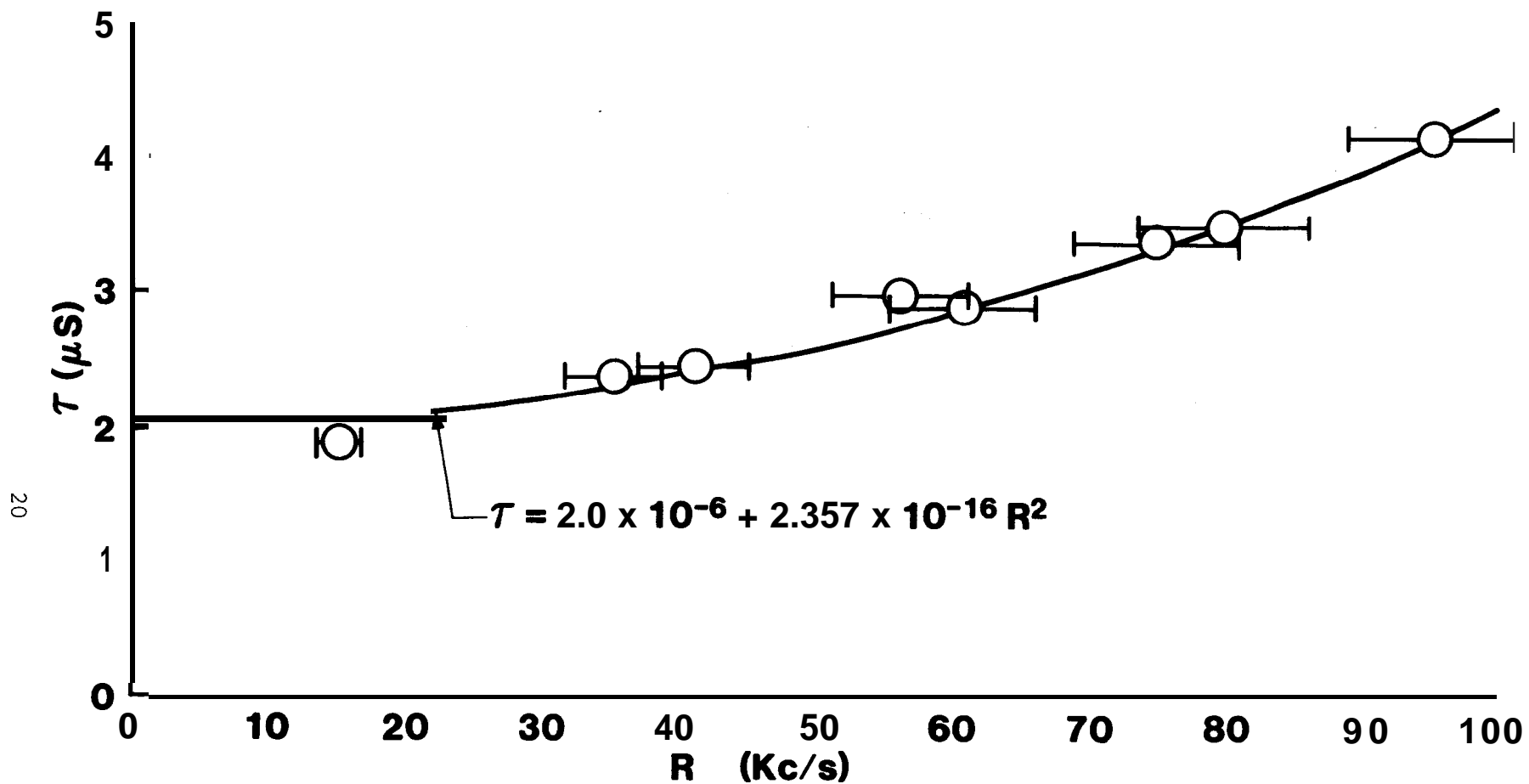


FIG. 5: System Time-Constant Calibration

In the present experiment (Fig. 2), all initial pathlengths and material attenuation coefficients would be previously measured. Thus, during the transient oil withdrawal, if an oil layer adhered to the cavity wall, then the one unknown would be the oil layer thickness (δ). However, if such a "protective" oil layer was not present ($\delta=0$), then the salt surface would undergo recession (ϵ), allowing this one unknown to be measured. Either δ or ϵ would be the length scale of interest, each occurring only in the absence of the other.

Certain criteria must be met for such measurements to be successfully made during transient oil withdrawal:

- (a) for $\epsilon > 0$, then $\mu_S \neq \mu_B$
 $(\delta = 0)$ I $\mu_B \approx \text{constant}$
- (b) for $\delta > 0$, then $\left\{ \begin{array}{l} \mu_O \neq \mu_B \\ \mu_B \approx \text{constant} \end{array} \right.$
 $(\epsilon = 0)$

Of these restrictions, $\mu_B \approx \text{constant}$ was most suspect, since significant density (specific gravity) variations with time would most likely occur at the fixed gamma-beam location during the transient oil withdrawal. "Bench-top" experiments were then undertaken, prior to building the apparatus of Fig. 2, in order to address this and related issues. Results of these pre-test experiments are discussed in the next section.

PRE-TEST RESULTS

Salt cores used throughout the present research were taken from deposits at Bryan Mound, Texas. This salt was found to possess 5% (by weight) insoluble materials. Two crude oils, possessing densities of 0.872 and 0.813 g/cc, were supplied for use.

Preliminary experiments were conducted during this phase of the research to investigate oil penetration into salt, as well as to quantify the thickness of any oil layer which might form on salt cavity surfaces during the proposed oil-withdrawal experiments. Two salt cylinders, each 5.08 cm in diameter by 15.24 cm in length, were machined from supplied salt cores. The first cylinder was placed in an existing autoclave and immersed in saturated brine at 13.9 MPa for 2 days, followed by immersion in crude oil at 13.9 MPa for 2 days. The second cylinder was immersed in oil only, at 13.9 MPa for 2 days. Photographs of post-test sections are shown in Fig. 6.

As can be seen, oil penetration into salt was found to be a strong function of conditions existing within the material's pore (or "grain boundary") space prior to its exposure to oil. In the first case, the pore volume was pre-flooded with saturated brine, effectively limiting subsequent oil penetration to the outermost regions of the sample (penetration depths of ≈ 0.6 to 0.7 cm). In the second case the pore volume was initially "dry", allowing the oil to completely flood the sample interior upon pressurization.

In these tests, as in the subsequent oil-withdrawal experiments, the salt samples were not mechanically loaded. Any existing micro-cracks and/or grain boundaries linking the exterior of the salt to its interior would thus remain open, providing favorable conditions for oil adherence/penetration. Should the oil fail to protect the salt from dissolution under these favorable (laboratory) conditions, it most certainly would exhibit the same inability in the field (salt in actual caverns being lithostatically loaded). Conversely, should the oil protect the unloaded salt from dissolution in the laboratory, extensions of such findings to the field would be uncertain. In that case, additional (more-complex) experiments would have to be performed using compressively-loaded salt samples.



(A) SATURATED BRINE (B) CRUDE OIL
137 ATM/2 DAYS; 137 ATM/2 DAYS.
CRUDE OIL
137 ATM/2 DAYS.

FIG. 6: Oil-Penetration Tests

Of the two fluid-penetration procedures summarized in Fig. 6, case A would be expected to produce salt samples which best simulated cavern conditions (i.e., salt preflooded with pressurized brine during cavern leaching, followed by exposure to pressurized oil during cavern filling). Case B would provide test samples most likely to result in the formation of a protective oil layer. Both procedures were used to prepare salt-cavity specimens prior to the transient oil-withdrawal experiments.

Oil-layer thicknesses on the salt cylinders were measured with the gamma-beam densitometer both before and after each pressurization cycle. Results showed $\delta \approx 0.3$ mm in all cases. No measurable reduction in count rate was observed during any of the pressurization cycles due to brine and/or oil penetration into the salt. This fact is consistent with the extremely low porosity of this material ($\approx .001$), which dictated that the maximum possible increase in path length of either fluid be equal to the product of the diameter times the porosity ($\approx .005$ cm), an immeasurable change.

Finally, linear attenuation coefficients for salt, crude oil, and brine (the latter as a function of dissolved salt content) were measured with the gamma-beam system. These substances were found to possess "sufficiently-different" μ values, as required for oil-withdrawal data interpretation/analysis. However, the attenuation coefficient for brine was found to be a linear function of dissolved salt content, showing an $\approx 18\%$ increase from the distilled-water limit to the fully-saturated-brine limit, consistent with a theoretical increase of $\approx 20\%$ for maximum dissolution of pure NaCl in pure H_2O . Consequently, two unknowns appear in the exponential attenuation equation, δ or ϵ , and μ_B . A requirement to independently measure salinity at the gamma-beam location thus seemed apparent.

Computer simulations of the proposed oil-withdrawal experiments were then undertaken (recall the geometry of Fig. 2). The gamma-beam equations, along with measured attenuation coefficients and postulated initial dimensions for the materials of interest, were input to SANSMIC. Three cases for the onset of salt dissolution at the gamma-beam location were considered: (1) no time delay (i.e., the salt wall begins to dissolve instantaneously

after oil/brine interface passage), (2) infinite time delay (i.e., oil-layer adherence protecting the salt from dissolution for all time), and (3) finite time delay (i.e., the oil layer "peels away" at some finite time after interface passage, allowing dissolution to begin). Fluid flow rates and withdrawal times were the same for all three cases.

Salt-wall recession and brine salinity distributions were predicted as functions of X and t for all locations beneath the upward-moving oil/brine interface. (Note: at any X and t , the code assumes brine salinity to be uniform across the cavity core, consistent with the turbulent, "fully-mixed" plume model^{12,13}. Further, since gamma-beam attenuation is a function of the integrated path length traversed; the thickness of the concentration boundary layer on each cavity wall was assumed to be negligible compared to the overall cavity diameter.) These predictions were then converted to predicted $R(t)$ responses at a fixed gamma-beam location (chosen to be "midway" between the initial and final interface locations). Figure 7 shows a schematic representation of these predicted $R(t)$ responses for the two limiting cases (no delay vs. infinite delay). Physical mechanisms which dictated these responses are reviewed below.

Consider first the "no delay" case. At $t = 0$, fresh-water injection was initiated below the brine/oil interface, causing it to rise. As the oil adjacent to the salt wall moved upwards, the oil in contact with the salt instantly detached, exposing the salt to dissolution. Prior to interface passage, the count rate remained constant since no dissolution was occurring at the gamma-beam location. As the brine/oil interface passed the gamma-beam location, an abrupt reduction in beam intensity (and thus count rate) occurred (brine being more dense than oil, and thus a better attenuator). Salt-wall recession at the gamma-beam location started at this time.

During the time period between interface passage and the cessation of oil withdrawal, the predicted $R(t)$ response must be viewed in light of three mechanisms: (1) the continued addition of fresh water, (2) salt addition to this water from an ever-increasing exposed surface area, and (3) recession of the salt wall itself. Numerical calculations showed that during this period, the "competing" effects of fresh-water addition and salt dissolution

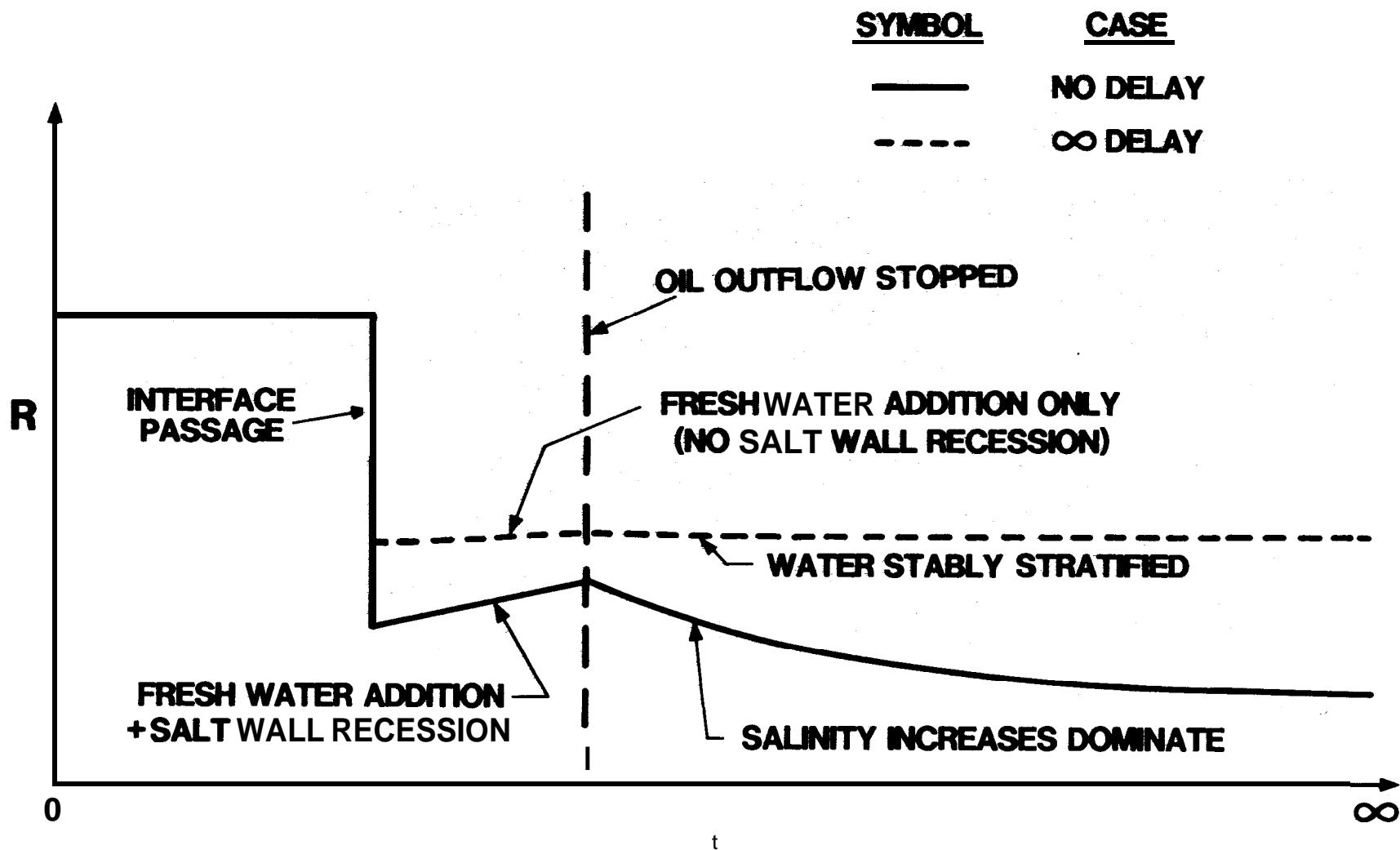


FIG. 7: Schematic of Predicted $R(t)$ Responses

into it approximately balanced, resulting in an essentially-constant brine salinity, and thus brine attenuation coefficient, at the gamma-beam location. Hence, in this portion of the proposed experiment, the predicted positive slope for $R(t)$ would be due primarily to the continued reductions in the pathlength of solid salt through which the beam must pass.

At some pre-selected time, oil withdrawal was terminated. The predicted $R(t)$ response was then seen to undergo an abrupt reversal in slope, from positive to negative, followed by an "exponential-like" decay to steady-state conditions. Calculations showed that following the cessation of fresh-water injection, overall beam attenuation would be dominated by brine. salinity increases over a large beam pathlength (the cavity diameter); the small additional reductions in the pathlength of solid salt predicted to occur during this period would have only a minor influence on $R(t)$. As the brine asymptotically approached a fully-saturated state, and the salt-wall recession rate went to zero, the slope of the $R(t)$ response likewise approached zero.

In contrast, consider now the other limiting case, an "infinite delay" time. As before, at $t = 0$, fresh-water injection was initiated below the brine/oil interface. In this case, however, a layer of oil adhered to the salt wall as the brine/oil interface rose, completely protecting all salt above the initial interface location from dissolution. Interface passage of the gamma-beam location again caused an abrupt reduction in beam intensity, but, in this case, to an R level measurably above that predicted to occur in the "no-delay" case. The reasons for this difference are twofold. The dominant reason was directly linked to the absence of salt dissolution at all locations above the initial interface location, i.e., the water at the gamma-beam location was predicted to be much less saline than before. A secondary reason was the fact that a finite-thickness layer of oil was assumed to adhere to "both sides" of the cavity, and $\mu_0 < \mu_B$. (Note: count rate levels predicted to occur for the infinite-delay case were found to be a weak function of assumed oil-layer thickness, δ , as will be demonstrated later.)

During the period between interface passage and the cessation of oil withdrawal, predicted count rates were seen to be essentially constant (the small increases in R being a direct result of the continued addition of fresh water, further reducing the already-low brine salinity). Upon the cessation of oil withdrawal, the only mechanism available to influence the predicted $R(t)$ response was molecular diffusion through a stably-stratified liquid (a process which occurs over an extremely long time scale compared to transient times of interest here). As a result, the predicted $R(t)$ curve remained at a quasi-steady-state level notably above that predicted to occur for the "no-delay" case. In quantitative terms, the count-rate difference between the two predicted steady-state levels was found to be ≈ 1000 counts/sec as compared to experimentally-observed uncertainties (statistical variations) in R of < 50 counts/sec.

Between these two limiting cases, an infinite number of finite-delay-time solutions exist. Numerical simulations showed that oil-layer "detachment" (and thus the onset of salt dissolution) after some finite-time delay would result in a rapid increase in brine salinity at the gamma-beam location. Beam attenuation would thus abruptly increase, resulting in a clearly-defined "transition" in the $R(t)$ response (i.e., an abrupt change from the plateau-like response of the infinite delay case to the exponential-like decay witnessed in the zero-delay case).

In summary, these computer simulations showed that the "shape" and "level" of the measured $R(t)$ response could be used to define the presence, or absence, of a protective oil layer during the transient oil-withdrawal process. Independent measurements of brine salinity at the gamma-beam location were, in fact, not required. Corroborating physical evidence to support conclusions reached in this manner would be sought from post-test sectioning and examination of each salt cavity tested.

The experiment thus appeared feasible and the apparatus of Fig. 2 was built.

EXPERIMENTAL RESULTS

Figure 8 shows a photograph of the traversable gamma-beam densitometer, and the test vessel, used in the present research. The source and detector vaults were mounted on opposite sides of a U-shaped, vertically-traversable platform. The gamma-beam path from source exit to detector entrance was accurately aligned upon system assembly, and thereafter remained invariant. The platform was positioned so as to straddle the test chamber, itself held in a separate support/alignment mechanism rigidly mounted to the laboratory wall. The test vessel centerline was accurately aligned with the beam path through vernier adjustments on both the test-chamber and platform mechanisms. Once aligned, the gamma beam could then be traversed along the entire vertical axis of the experiment (maximum system traverse of ≈ 80 cm, with an absolute location accuracy of $\pm .005$ cm, as defined by laser time-of-transit calibrations). The platform drive mechanism and the counting electronics were both linked to a microcomputer, thereby allowing a preprogrammed sequence of beam locations and data-acquisition times to be implemented. Resulting $R(X)$ and $R(t)$ files were both printed and stored for subsequent analyses.

Figure 9 shows a photograph of a salt-cavity test specimen. The internal surfaces of each cavity were "preconditioned" via a 30-second exposure to fresh water in order to remove the "as-machined" surface finish. All dimensions of the test sample were then measured (via micrometer) prior to its placement in the pressure vessel. Saturated brine and crude oil were then introduced into the cavity according to one of the impregnation cycles described earlier (Fig. 6). Table 1 summarizes the test conditions utilized during each of the four separate oil-withdrawal experiments that were conducted.

It should be noted that present test conditions were consistent with criteria reported by Saberian⁷ for the attainment of a turbulent injection plume and turbulent natural convection in the wall boundary layer. Oil/brine interface velocities bracketed values proposed for actual field operations. The imposed pressure was consistent with actual cavern levels and all experiments were run at a constant temperature of 23°C.

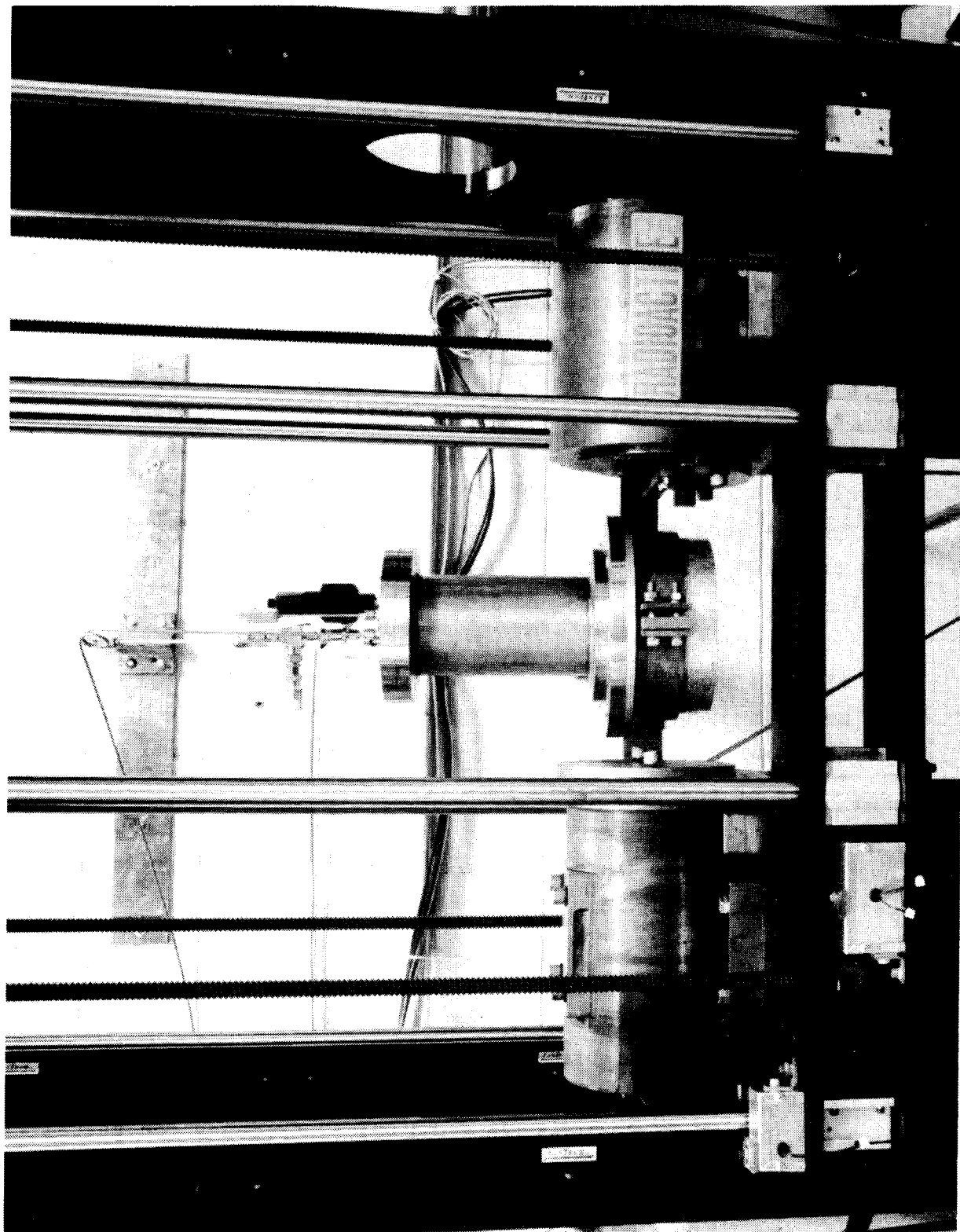


FIG. 8: Photograph of Gamma-Beam System and Test Vessel



FIG. 9: Photograph of Salt Cavity Model

SUMMARY OF TEST CONDITIONS



| EXP. | PRESSURIZATION HISTORY (FLUID/ATM./DAYS) | ρ_o (g/cc) | $X_{l,i}$ (IN.) (cm) | \bar{Q}_{WD} (cc/min.) | t_{WD} (min.) | $X_{l,f}$ (IN.) (cm) | \bar{U}_l (m/hr.) |
|-------------|--|--------------------|----------------------------|-----------------------------|--------------------|----------------------------|---|
| SPR 1 | SAT. BRINE/ 137/2 OIL/137/2 | .872 | 1.45 (3.68) | 2.86 | 90 | 6.41 (16.28) | .084 |
| SPR2 | SAT. BRINE/ 137/2 OIL/137/2 | .813 | 1.45 (3.68) | 12.95 | 22 | 6.94 (17.62) | ●  |
| SPR3 | SAT. BRINE/ 137/2 OIL/ 137/2 | .813 | 0.90 (2.29) | 32.44 | 9 | 6.53 (16.59) | .953 |
| SPR4 | OIL/137/2 | .813 | 1.30 (3.30) | 14.84 | 19 | 6.71 (17.04) | ■  |

TABLE 1

In this report, detailed results from experiment SPB2 will be shown as representative of all four experiments, in that all four yielded the same basic $R(t)$ response. Consequently, all four experiments support the same conclusion, independent of pressurization history, oil density, initial interface location, and interface velocity.

Figure 10 shows the "initial" count-rate scan for SPR2, plotted versus the gamma-beam coordinate, x_γ . This distribution was measured after the stated pressurization history and immediately prior to oil withdrawal. Two "plateaus," one for the saturated-brine pocket and one for the overlying crude oil, are evident. These two regions are separated by a steep linear increase in count rate, "spread" over several beam diameters, the center of this ramp defining the initial interface location. This initial $R(x_\gamma)$ scan was analyzed, via the exponential attenuation law for the system, to solve for $\mu_s(x_\gamma)$, the attenuation coefficient distribution for the salt sample. Such distributions did show spatial non-uniformities, consistent with the material's geologic origin.

The precise location of both the cavity bottom and top were "masked" by an increase in beam attenuation due to the vessel flanges (note the drop-offs in R at each end of this measured distribution). This experimental limitation necessitated a separate coordinate-calibration experiment. In this calibration, an aluminum test specimen, which possessed dimensions identical to the salt-cavity models, was used. Grooves of known dimensions, at known distances from the cavity bottom, were machined into the metal. A scan of this model (positioned inside the pressure vessel) yielded the required relationship between X and x_γ , namely $X = x_\gamma - 5.84$ cm. The initial location of the interface relative to the cavity bottom was thus precisely defined.

Figure 11 shows the transient $R(t)$ response for SPR2, as measured at a station 10.03 cm from the initial cavity bottom. All the characteristic features of a "no-delay" response are clearly evident (recall the schematic of Fig. 7). The crude oil did not protect the salt from dissolution

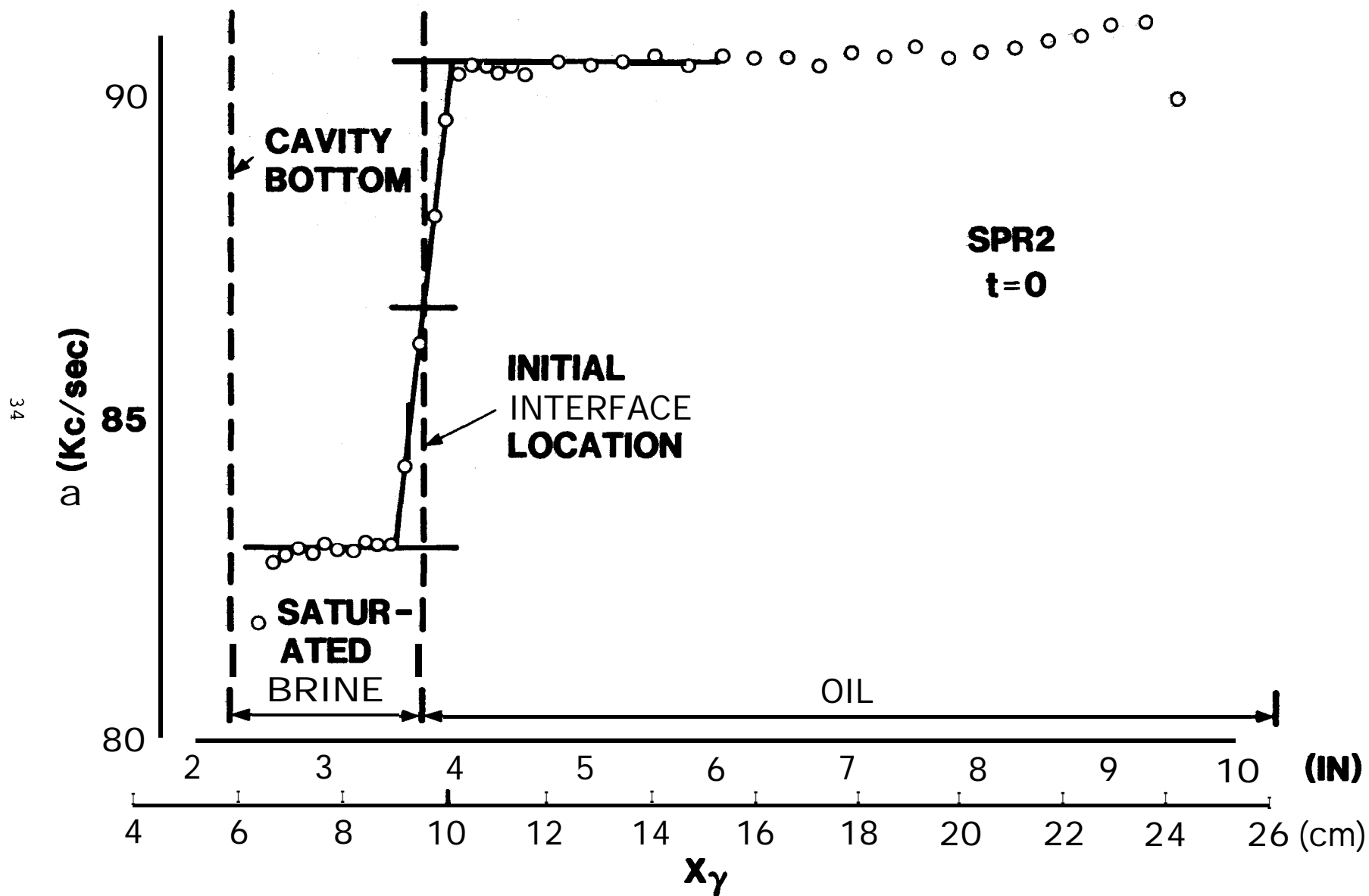


FIG. 10: Measured Count-Rate Distribution, SPR2, t=0

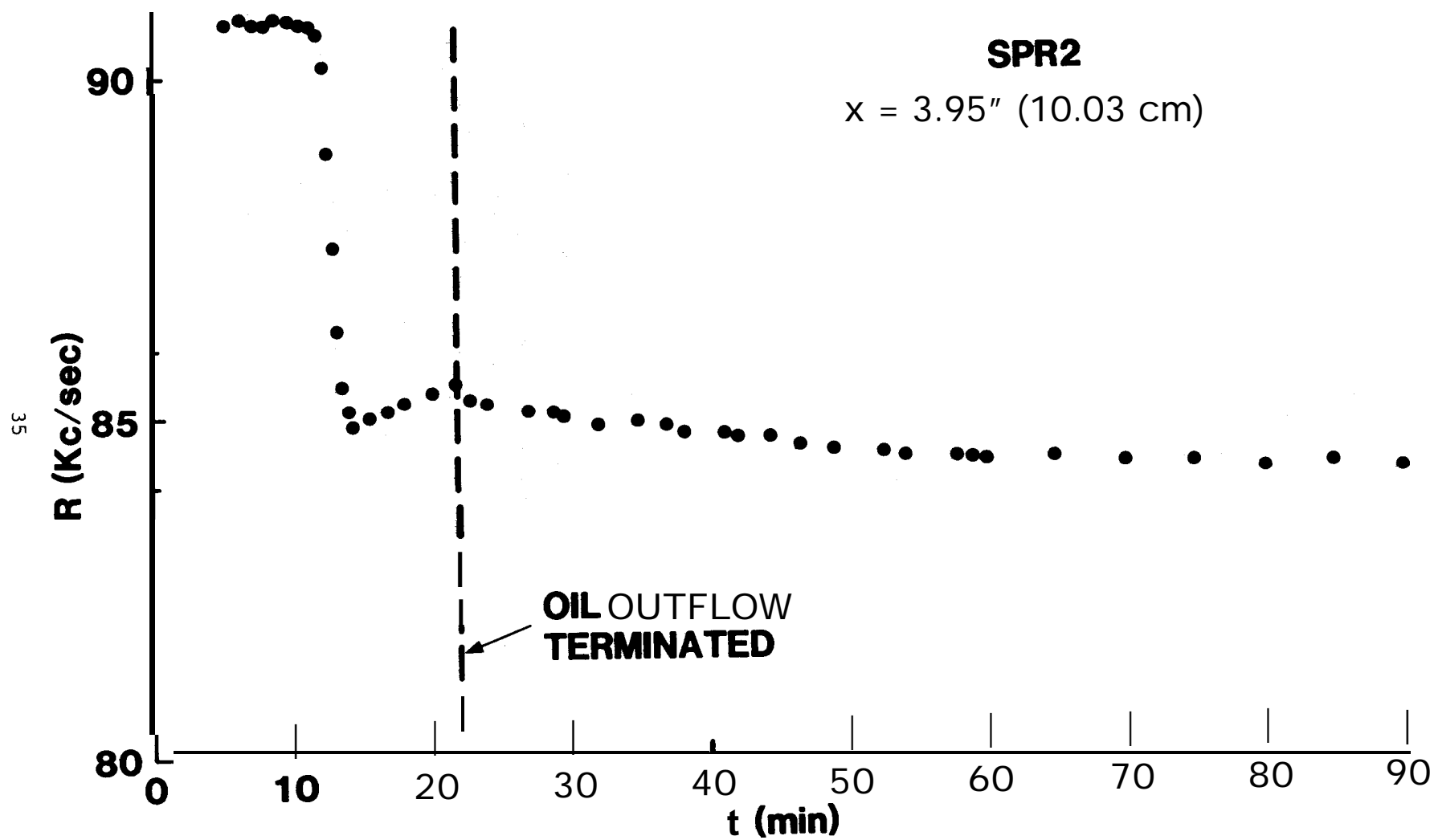


FIG. 11: Measured Transient Count-Rate Response, SPR2, $X=10.03 \text{ cm}$

following interface passage. Comparisons of experimental results with numerical predictions will be shown in the next section.

Figure 12 shows the measured post-test (equilibrium) count-rate distribution for SPR2. (Note: to ensure saturated-brine conditions, final scans were taken approximately twenty-four hours after the cessation of oil withdrawal.) Shown for reference are the initial cavity bottom, the initial and final interface locations, and the pre-withdrawal count-rate level (as measured through saturated brine and the initial thickness of solid salt). (Note: the final interface location could not be inferred directly from this measured $R(X)$ distribution due to "flange masking" of the signal, as discussed earlier. Hence, it was calculated based on the measured volume of oil recovered from the cavity, accounting for compressibility effects.)

As can be seen in Fig. 12, measured post-test count rates, at all locations beneath the final oil interface, were found to be greater than the pre-test level. Since the liquid internal to the cavity, and below the oil, was saturated brine in both cases, these increased count rates could only be attributed to a reduction in the thickness of solid salt (i.e., salt-wall recession occurred at all locations exposed to unsaturated brine during the oil-withdrawal process). Having previously measured the $\mu_s(X)$ distribution, this post-test $R(X)$ distribution was then used to solve the attenuation equation for $\epsilon(X)$, and thus the final cavity shape (results to be shown below).

Figure 13 shows a post-test, sectioned view of the SPR2 salt cavity. Some asymmetry (preferential pitting) was observed, possibly due to non-uniform deposits of solubles other than NaCl. By measuring the outer diameter of the cylindrical sample both before and after sectioning, the cut-plane thickness was determined. Radial distances (depths) from the cut plane surface to the cavity wall were measured as a function of X along the centerline of each cavity half. These radial depths were added to one-half the cut-plane thickness, then averaged, to derive a final cavity shape, $r(X)$.

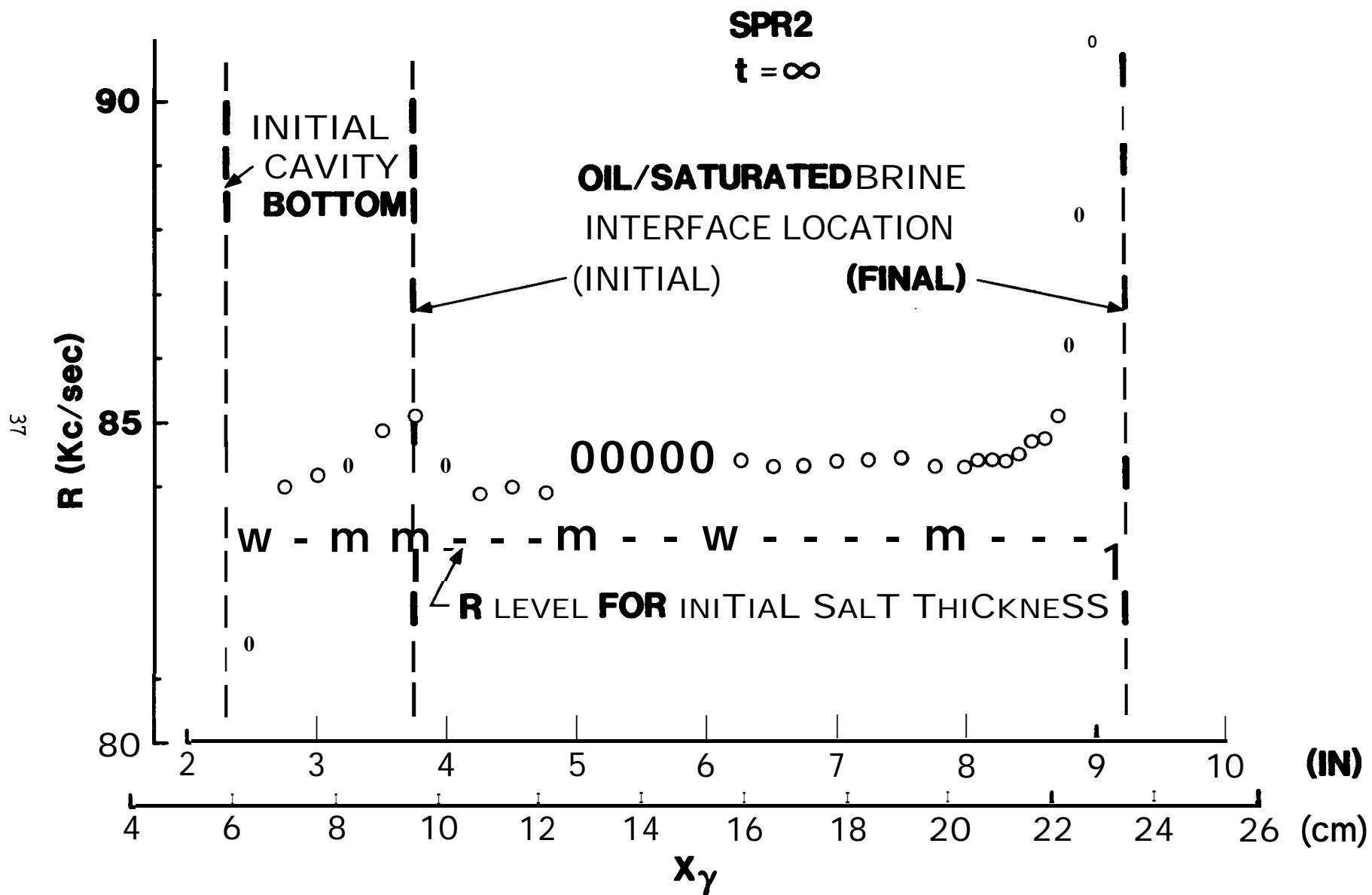


FIG. 12: Measured Count-Rate Distribution, SPR2, $t = \infty$

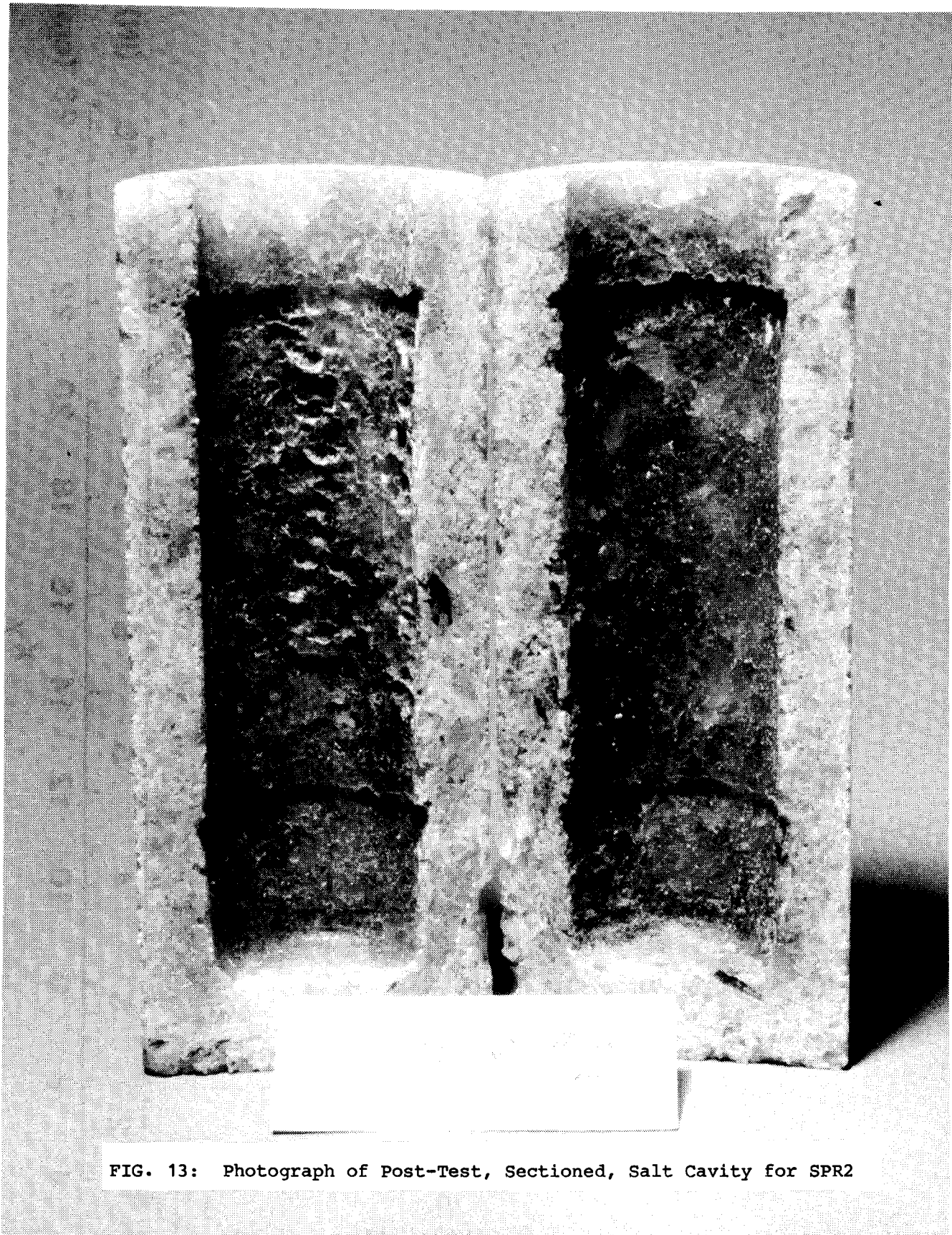


FIG. 13: Photograph of Post-Test, Sectioned, Salt Cavity for SPR2

Figure 14 shows a comparison of final cavity shapes, as measured both by sectioning and by the gamma-beam system. The radial scale has been magnified by a factor of five over the vertical scale to better illustrate cavity features. Agreement between these two measurement techniques is seen to be excellent, proving that the gamma-beam technique can accurately measure cavity shape change.

As can be seen in Figs. 13 and 14, "undercuts" formed at both the initial and final interface locations. Both of these undercuts are attributed to the same basic phenomenon, fresh water rising vertically to its maximum allowable position (i.e., the overlying oil blanket) where it stagnated, preferentially etching the salt. On vessel pressurization to 13.9 MPa, the liquids in the cavity compressed, the solid salt compressed, and the test vessel expanded, all to a minor, but non-negligible extent, thereby allowing some small volume of fresh water to enter the vessel. Resultant salt dissolution at the initial interface location increased the cavity volume an incremental amount, allowing still more fresh water to enter. This sequence of events asymptotically ceased upon the attainment of equal pressures in the two vessels and the attainment of saturated-brine conditions within the salt cavity. Similarly, upon the abrupt cessation of oil-withdrawal, the final increment of injected fresh water was trapped beneath the overlying oil, etching the uppermost groove. Between these two interface locations, essentially uniform salt recession occurred.

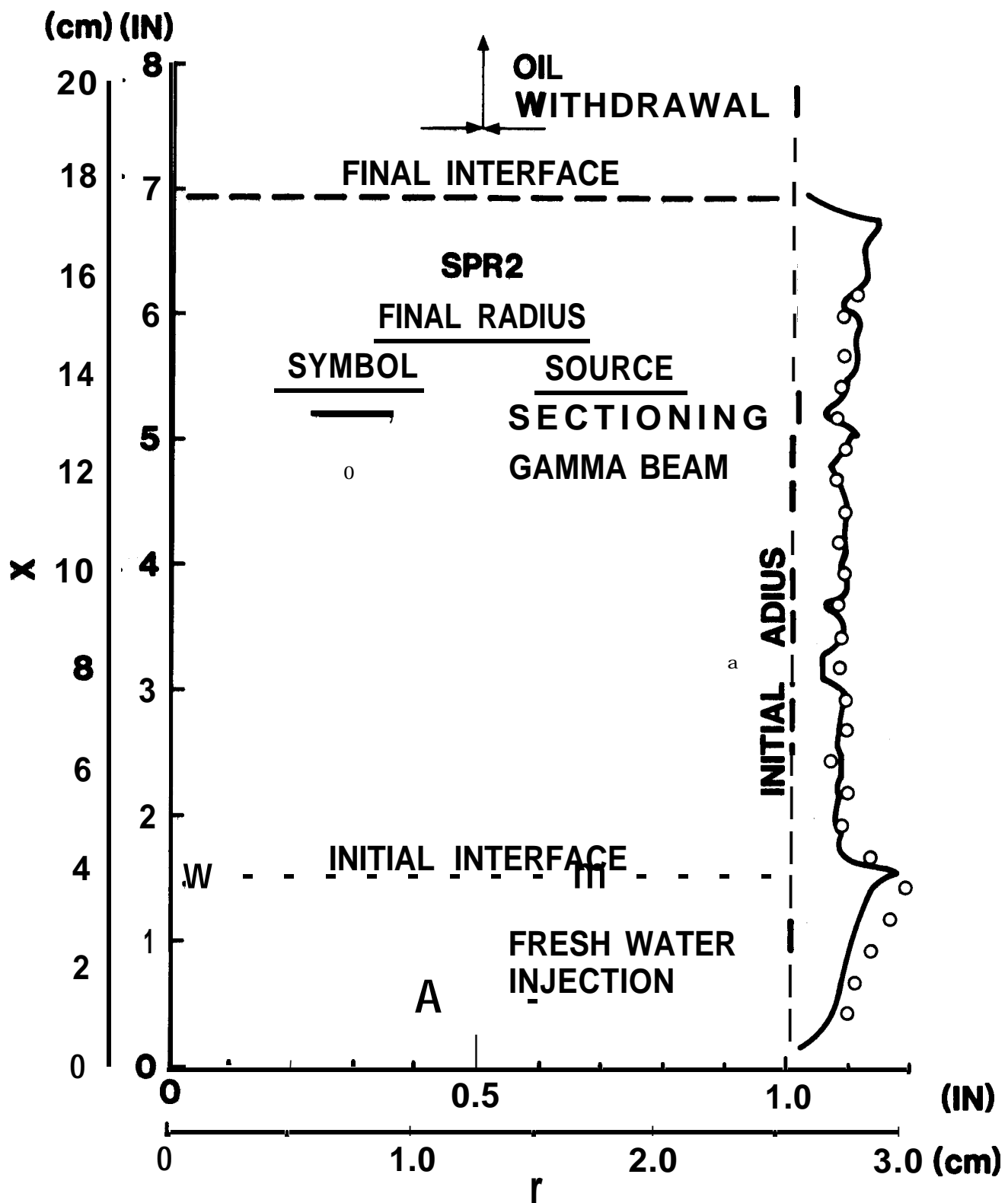


FIG. 14: Measured Post-Test Cavity Shape, SPR2

COMPARISONS WITH NUMERICAL PREDICTIONS

SANSMIC^{10,11} was used to generate numerical predictions for both the transient $R(t)$ response and the steady-state $r(X)$ shape for each oil-withdrawal experiment. Comparisons with the experimental results presented in the previous section are discussed here.

Figure 15 shows data comparisons with $R(t)$ predictions for the two limiting cases, no delay and infinite delay. The infinite-delay case was run for two assumed oil-layer thicknesses, one matching present gamma-beam measurements ($\delta = .03$ cm) and one a factor of 3.33 larger, in order to demonstrate the weak dependence of the predictions on this parameter. Although some minor discrepancies between the no-delay predictions and the data can be seen, overall agreement with this case is clearly evident. Between interface passage and the Cessation of oil withdrawal, the measurements exhibit a slightly-greater slope than the predictions. This difference is most likely a result of the modelling in the code which assumes a "fully-mixed" plume, and thus does not attempt to model radial variations in brine salinity. While such an assumption is justifiable on a cavern scale, such conditions may not have been achieved in the laboratory-scale experiments. In the present case, the core of the buoyant plume may have contained water of a somewhat lower salinity than the surrounding liquid, causing a path-length integrated beam attenuation somewhat less than predicted to occur under "fully-mixed" conditions. Immediately following the cessation of oil withdrawal, however, both the data and the predictions show an immediate, exponential-like decay to the same steady-state count rate, demonstrating excellent agreement with respect to total wall recession at the gamma-beam location.

Figure 16 shows a comparison of final cavity shapes, predictions having been made under the "no-delay" assumption. In order to model the "undercut" phenomenon which occurred during cavity pressurization, an injection of 10 cubic centimeters of fresh water into the brine pocket, followed by a 30 minute time delay, were specified prior to the onset of oil withdrawal. Total salt-wall recession everywhere above the initial interface location was well predicted, the only discrepancies occurring in the region

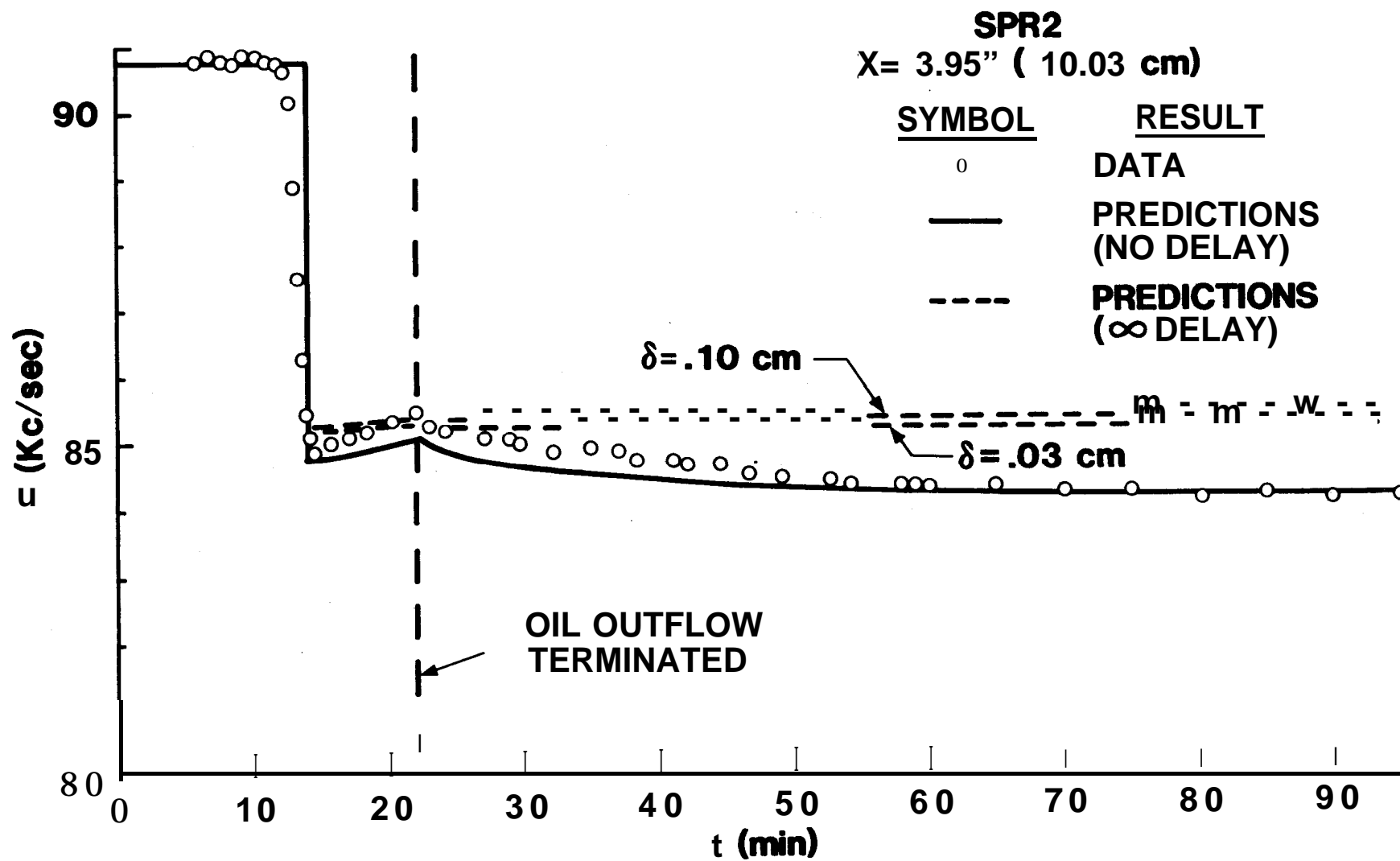


FIG. 15: Transient Count-Rate Response, SPR2, Data versus Predictions

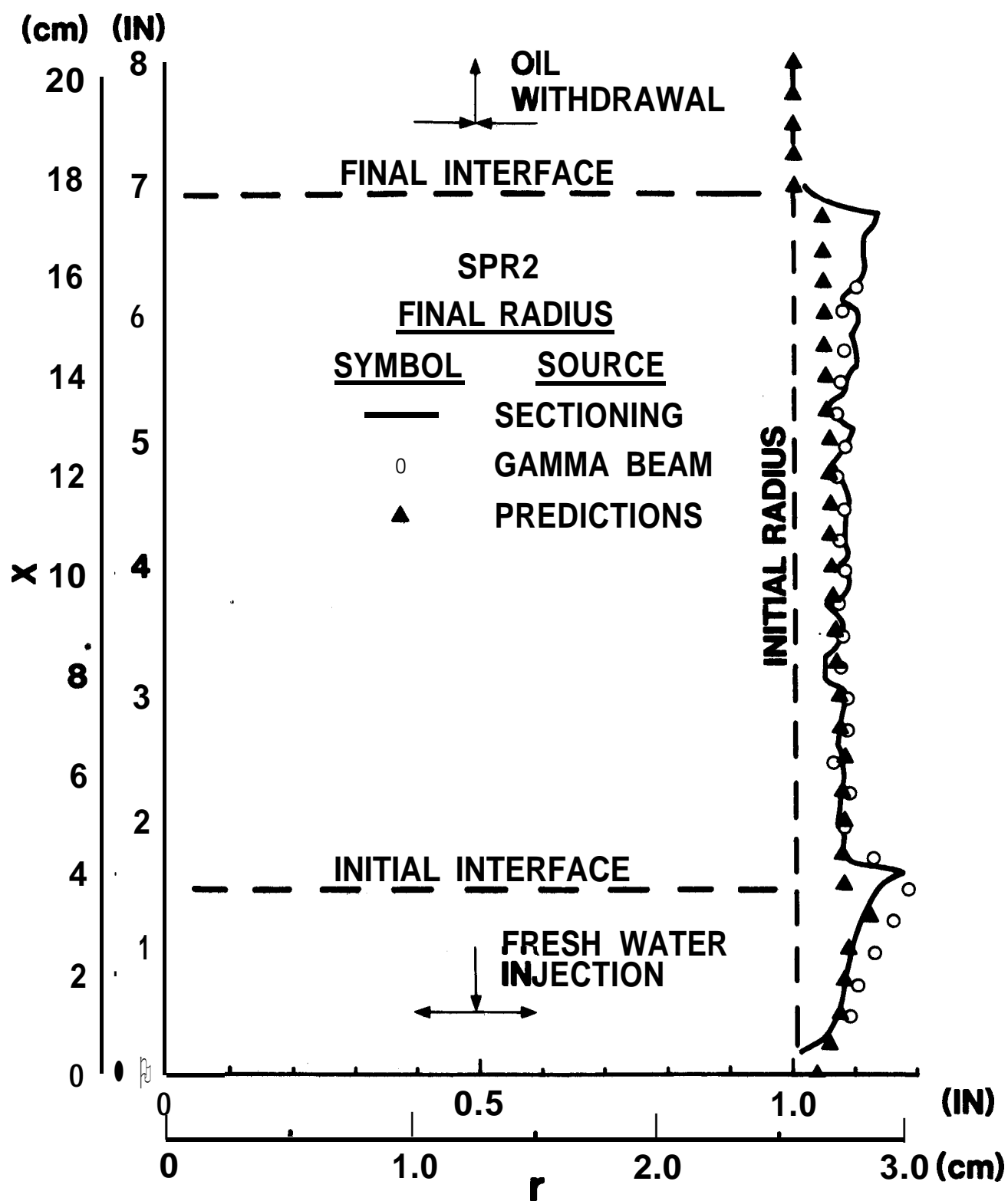


FIG. 16: Post-Test Cavity Shapes, **SPR2**, Data versus Predictions

immediately below the final **interface** location, where recession was underpredicted. This underprediction is attributed to "plume effects," large-scale **modelling** versus laboratory-scale experiments.

In order to expand further on this issue, three additional experiments were conducted to investigate salt-cavity leaching in the absence of any overlying crude oil (the only variable in these experiments being the relative vertical position of the injection and withdrawal lines). Transient and steady-state data for "**direct**" leaching (injection below withdrawal) and "**reverse**" leaching (injection above withdrawal), in comparison with **numerical** predictions, will be reported in **a** subsequent report¹⁵.

CONCLUSIONS

Oil/brine/salt interactions were experimentally investigated in the laboratory in support of the U.S. Strategic Petroleum Reserve program. As a result of these experiments, and through comparisons with numerical predictions, the following observations were made:

1. Oil layer adherence, and/or penetration, did not protect salt surfaces from dissolution following oil/brine interface passage. Therefore, the oil-withdrawal technique studied here, when applied in actual field operations, should not adversely affect cavern shape change.

2. Measured and predicted post-test cavity shapes were found to be in good agreement, further validating the SANSMIC code^{10,11} for use in SPR program applications.

REFERENCES

1. Durie, R. W. and Jessen, F. W., "Mechanism of the Dissolution of Salt in the Formation of Underground Salt Cavities," **Soc. Petroleum Engineers Journal**, June, 1964, pp. 183-190.
2. Durie, R. W. and Jessen, F. W., "The Influence of Surface Features in the Salt Dissolution Process," **Soc. Petroleum Engineers Journal**, September, 1964, pp. 275-281.
3. Kazemi, H. and Jessen, F. W., "Mechanism of Flow and Controlled Dissolution of Salt in Solution Mining," **Soc. Petroleum Engineers Journal**, December, 1964, pp. 317-328.
4. Jessen, F. W., "Total Solution Mechanism," **AIME Transactions**, Vol. 250, December, 1971, pp. 298-303.
5. Von Schonfeldt, H., "Model Studies in Solution Mining," **Proc. 4th International Symposium on Salt**, N. Ohio Geologic Society, Houston, TX, 1973.
6. Chang, C., Vliet, G. C. and Saberian, A., "Natural Convection Mass Transfer at Salt-Brine Interfaces," **Journal of Heat Transfer**, Vol. 99, November 1977, pp. 603-608.
7. Saberian, A. and Podio, A. L., "A Computer Model for Describing the Development of Solution-Mined Cavities," **IN SITU**, 1(1), 1977, pp. 1-36.
8. Pottier, M. and Esteve, B., "Simulation of Gas Storage Cavity Creation by Numerical Methods," **Proc. 4th International Symposium on Salt**, N. Ohio Geologic Society, Houston, TX, 1973.
9. Nolen, J. S., et al, "Numerical Simulation of the Solution Mining Process," **Soc. of Petroleum Engineers**, SPE-4850, European Spring Meeting, Amsterdam, The Netherlands, May, 1974.
10. Russo, A. J., "A Solution Mining Code for Studying Axisymmetric Salt Cavern Formation," **Sandia National Laboratories Technical Report**, SAND81 - 1231, September 1981.

11. Russo, A. J., "A User's Manual for the Salt Solution Mining Code, SANSMIC, " Sandia National Laboratories Technical Report, SAND83-1150, September 1983.
12. Morton, B. R., Taylor, G., and Turner, J. S., "Turbulent Gravitational Convection from Maintained and Instantaneous Sources," **Proc. Royal Society, Series A**, Vol. 234, No. 1196, January 1956, pp. 1-23.
13. Turner, J. S., "Buoyancy Effects in Fluids," Cambridge University Press, New York, NY, 1973.
14. Reda, D. C., Hadley, G. R. and Turner, J. A., 'Application of the Gamma-Beam Attenuation Technique to the Measurement of Liquid Saturation for Two-Phase Flows in Porous Media," **Proc. of the 27th International Instrumentation Symposium, Instrument Society of America, Indianapolis, IN, April 1981**, pp. 553-568.
15. Reda, D. C. and Russo, A. J., "Experimental Studies of Salt Cavity Leaching via Fresh-Water Injection," Sandia National Laboratories Technical Report, SAND84-0020, to be printed, 1984.

Distribution:

E. E. Chapple, PMO-681 (6)
U. S. DOE SPRPMO
900 Commerce Road East
New Orleans, LA 70123

L. Rousseau
U. S. DOE SPRPMO
900 Commerce Road East
New Orleans, LA 70123

V. Kilroy
U. S. DOE SPRPMO
900 Commerce Road East
New Orleans, LA 70123

Larry Pettis
U. S. Department of Energy
Strategic Petroleum Reserve
1000 Independence Avenue, SW
Washington, DC 20585

Bill Wilson
U. S. Department of Energy
Strategic Petroleum Reserve
1000 Independence Avenue, SW
Washington, DC 20585

Aerospace Corporation (2)
800 Commerce Road East, Suite 300
New Orleans, LA 70123
Attn: E. Katz
R. Merkle

Jacobs/D'Appolonia Engineers(2)
P. O. Box 23308
Harahan, LA 70183
Attn: P. Campbell
H. Kubicek

POSSI (2)
850 S. Clearview Pkwy.
New Orleans, LA 70123
Attn: Dub Butler
K. E. Mills

W. Marquardt
Parsons-Gilbane
800 Commerce Road West
New Orleans, LA 70123

Alfred H. Medley
Fenix & Scisson, Inc.
1401 South Boulder
Tulsa, OK 74119

Dr. Alfred Finkenwirth
LANZSTR.25
6200 Wiesbaden
West Germany

Gayle D. **Petrick**, P.E.
Diamond Crystal Salt Company
St. Clair, MI 48079

Eng. Diamantino Mendonca
Socio-Gerente
Sondagens E. **Fundacoes A. Cavaco, LDA.**
Av. Eng. Durate Pacheco, 21-2.º
1000 Lisbon
Portugal

Ir. Th. H. Wassmann
Manager, Minerals Department
Akzo Zout **Chemie** Nederland bv
Boortorenweg 20
7554 RS Hengelo (O)
The Netherlands

Jerome S. Blank
Kalium Chemicals
Suite 1120
600 South Cherry Street
Denver, CO 80222

Joseph Didier Martinez, CPGS, PE
P. O. Drawer J.D.
University Station
Baton Rouge, LA 70893

Elmar L. Goldsmith
Kalium Chemicals
400 Bank of Canada Building
Regina, Saskatchewan S4P 0M9
Canada

Hans Y. Tammemagi, PhD
RE/SPEC Ltd.
4616 Valiant Drive, NW - Suite 201
Calgary, Alberta T3A 0X9
Canada

Hans-J. Doering
RuhrgasAktiengesellschaft
Referent Technische Planung - Lagerstätten
Huttropstrasse 60
D-4300 Essen 1
West Germany

Dr. Adrian J. Van Der Hoeven
Nord-West Kavernengesellschaft
MIT Beschränkter Haftung
2940 Wilhelmshaven 31
Kavernenfeld K-6
West Germany

James H. Huizingh
Texasgulf Chemicals Co.
P. O. Box 1208
Moab, UT 84532

E. Leon Cook
PPG Industries, Inc.
P. O. Box 1000
Lake Charles, LA 70602

Diamond Shamrock Corp.
P. O. Box 1000
Pasadena, TX 77501
Attn: R. G. LaFortune

A. Saberian and Associates
3305 Northland Drive #407
Austin, TX 78731

Solution Mining Research Center (50)
812 Muriel St.
Woodstock, IL 60098
Attn: H. W. Fiedelman

PB-KBB, Inc. (2)
11999 Katy Freeway, #600
P. O. Box 19672
Houston, TX 77024
Attn: W. M. Bishop
R. W. Blair

1510 J. W. Nunziato
1511 G. G. Weigand
1512 J. C. Cummings
1512 D. C. Reda (25)
1512 A. J. Russo
1513 D. W. Larson
1513 R. J. Gross
1520 D. J. McCloskey
1530 L. W. Davison
1540 W. C. Luth
6257 J. K. Linn (6)
3141 C. M. Ostrander (5)
3151 W. L. Garner (3)
for DOE/TIC (Unlimited Release)
3154-3 C. H. Dalin (25)
DOE/TIC
8424 M. A. Pound